Microporous and Mesoporous Materials 155 (2012) 47–55

Contents lists available at SciVerse ScienceDirect

Microporous and Mesoporous Materials

journal homepage: www.elsevier.com/locate/micromeso

Characterization of a monolithic mesoporous carbon as diffusion layer for micro fuel cells application

Yohann R.J. Thomas [a], Mariano M. Bruno [a,b], Horacio R. Corti [a,c,*]

[a] Departamento de Física de la Materia Condensada, Centro Atómico Constituyentes, Comisión Nacional de Energía Atómica (CNEA), General Paz 1499 (1650) San Martín, Buenos Aires, Argentina
[b] Escuela de Ciencia y Tecnología, Universidad de Gral. San Martín, Martin de Irigoyen 3100 (1650), San Martín, Buenos Aires, Argentina
[c] Instituto de Química Física de los Materiales, Medio Ambiente y Energía (INQUIMAE), Universidad de Buenos Aires – CONICET, Ciudad Universitaria, Pabellón II, 1428 Buenos Aires, Argentina

ARTICLE INFO

Article history:
Received 17 October 2011
Received in revised form 25 December 2011
Accepted 7 January 2012
Available online 16 January 2012

Keywords:
Mesoporous carbon
Micro fuel cells
Diffusion layer
Contact resistance
Permeability

ABSTRACT

The preparation and characterization of a monolithic mesoporous carbon structure, which could be used as diffusion layer in PEM and DMPEM micro fuel cells, is described. Several characteristics of the monolithic carbon were studied, such as specific surface area, pore size distribution, bulk electrical resistivity, contact resistance with graphite plates, along with the wettability, imbibition and permeability of methanol aqueous solution. These properties were compared to those reported for commercial carbon paper and carbon cloth materials commonly used as diffusion layers in PEM fuel cells. The electrical properties of the mesoporous carbon meet the requirements to be employed as diffusion layers in PEM stacks assembled at pressures above 15 bar. The rapid spreading and imbibition of concentrated methanol solutions in the mesoporous carbon, as well as the permeability of the aqueous methanol through it, also make this mesostructured carbon a possible candidate for diffusion layer and catalyst support in passive direct methanol micro fuel cells.

1. Introduction

The increasing demand for reliable power sources in today's power hungry portable electronics has promoted the development of integrated systems for micro fuel cells feed with hydrogen or methanol [1–5]. Carbon materials are some of the key components of these micro systems, being part of the catalyst support, the diffusion layer (DL) and the bipolar plates (BPs). The use of different new types of nanostructured carbon materials, including ordered mesoporous carbon (OMC), in catalyst is recognized [6] and their applications in fuel cells has been reviewed by Chang et al. [7], who predicted catalyst loads higher than 90 wt% on OMC.

For instance, the successful application of nanostructured carbon, prepared using silica or zeolite as a template, as catalyst support for cathode proton exchange membrane (PEM) fuel cells [8], or as electrode for methanol oxidation [9] has been reported. We have also probed that monolithic mesoporous carbon (MMC) with hierarchical pore structure [10] can be also used as substrate in the electrodeposition of Pt catalysts for methanol oxidation [11], and the grinded material was used as methanol tolerant catalyst support for the oxygen reduction reaction [12].

Gas diffusion layers (GDLs), typically carbon paper or carbon cloth, is a critical component of H_2/air PEM fuel cells [13] because its properties determine the contribution to the ohmic and mass transport losses. In the case of direct methanol fuel cells (DMFCs) the transport of methanol towards the anode is hindered by the formation of carbon dioxide bubbles. Thus, the two-phase transport in the anode DL is a critical factor in this type of cells, which requires the use of Teflon® [14] to regulate the hydrophobicity and avoid flooding. On the other hand, the inclusion of a microporous layer on the cathode DL has been shown to improve the oxygen transport [15,16]. Mesoporous carbon (MC) with hierarchical pore structure, that is, having a coarse structure in the interior and microstructured top and bottom layers, has been used by Glora et al. [17] to improve the contact resistance between the gas diffusion electrodes and the membrane.

The preparation and characterization of different types of mesoporous carbon, including OMC [18], mesoporous carbon/carbon composites [19], sol–gel prepared [20] and soft-templating prepared [21–23] materials have been described in the recent literature, although few studies report the characterization of the mesoporous carbon as DL in fuel cell, or analyze the relevant physical and chemical properties they should meet for its use in fuel cells.

* Corresponding author at: Departamento de Física de la Materia Condensada, Centro Atómico Constituyentes, Comisión Nacional de Energía Atómica (CNEA), General Paz 1499 (1650) San Martín, Buenos Aires, Argentina. Tel.: +54 11 6772 7174; fax: +54 11 6772 7121.
E-mail address: hrcorti@cnea.gov.ar (H.R. Corti).

1387-1811/$ - see front matter © 2012 Elsevier Inc. All rights reserved.
doi:10.1016/j.micromeso.2012.01.012

The comprehensive characterization of DL for PEM fuel cells comprises: bulk (in- and through-plane) electrical resistivity, contact resistance with BP, gas permeability, pore size distribution, and surface morphology [13,24], while liquid permeability, wettability and imbibition are relevant for DMFC. It is also important to analyze how these properties change upon compression forces, as those present in the assembled fuel cell stack [25]. The characterization in fuel cell operation conditions is the most astringent test for a new DL material [25,26], but the above mentioned properties should be optimized if a good fuel cell performance is expected.

In this work we synthesized, using the soft template method, a MMC having a moderate specific area and a well defined pore size distribution. Several features of the material, such as electrical resistivity, contact resistance, aqueous methanol permeability, liquid wettability and imbibition have been also analyzed in relation to its application in direct methanol fuel microcells.

2. Experimental

2.1. Mesoporous carbon preparation

Mesoporous carbon support was obtained using the method described elsewhere [10,27]. Briefly, the precursor was prepared by polymerization of resorcinol (Fluka) and formaldehyde (Cicarelli, 37 wt%), using sodium acetate (Cicarelli) as catalyst and the cationic polyelectrolyte poly(diallyldimethylammonium chloride), (PDADMAC, Sigma–Aldrich) as a structuring agent. The reactive mixture of resorcinol (R), formaldehyde (F) and sodium acetate (C) in aqueous solution at 40 °C, was stirred for 10 min and finally the PDADMAC (P) was added. The molar ratios of the components R:F:C:P were: 1:3:0.016:0.0212, respectively, where the monomeric unit was used for P. Once the mixture becomes homogenous, the solution was heated at 70 °C for 48 h at atmospheric pressure. The brown monolithic RF polymer obtained was dried in air for 3 days. The resulting material was finally carbonized under nitrogen in a tubular furnace. The sample was heated, at a rate of 60 K h^{-1}, from ambient temperature up to 800 °C (named MC800) or up 1000 °C (named MC1000) in order to analyze the effect of the thermal treatment on the carbon properties. The monolithic samples can be prepared in different sizes because the colloidal solution is poured into a mould before gelation and curing. In this work square plates about 2 cm × 2 cm, with typical thickness between 200 and 400 μm, were used.

Mesoporous carbon having capillaries of about 15 μm in diameter were also prepared using polypropylene cloth as a hard template in addition to the PDADMAC (soft templates) using the procedure described previously [10]. The resin with both templates was carbonized at 800 °C (MC800/wC) or 1000 °C (MC1000/wC).

Commercial GDLs were also used for comparison with the MC: Toray® TGP-H-060 and TGP-H-090, which are carbon papers without hydrophobic treatment (0% teflonized) with thickness of 190 and 280 μm, respectively, and carbon cloth AvCarb 1071 HCB, 380 μm in thickness.

2.2. Carbon characterization

2.2.1. Morphological characterization

The surface area of the carbon was calculated from the measured nitrogen adsorption isotherms at 77 K (Micrometrics ASAP2020) using the Brunauer–Emmett–Teller (BET) equation [28]. The microporous fraction was evaluated using *t*-plot, and the pore size distribution (PSD) was calculated using (N_2) original density functional theory (DFT) software from Micromeritics, applying slit pore geometry.

After the carbonization process, the material was observed by a scanning electron microscope (SEM) – FEI Company (Quanta 200). The roughness of the samples was determined with a surface profiler (Form Talysurf 50, Taylor Hobson) and AFM (Veeco-DI Multimode Nanoscope IIIa).

2.2.2. Electrical in-plane resistivity

The electrical in-plane resistivity of our material was determined using the van der Pauw method [29], which is a four probes ASTM standard procedure for resistance measurement that eliminates errors due to contact resistance [30]. The electrical resistivity, ρ, of the sample was obtained from the expression [29]:

$$\rho = \frac{\pi\delta}{\ln 2}\frac{(R_{AB,CD}+R_{BC,DA})}{2} f\left(\frac{R_{AB,CD}}{R_{BC,DA}}\right) \quad (1)$$

where δ is the thickness of the sample, $R_{AB,CD}$ is the resistance calculated as the ratio of the current, measured between the probes A and B, and the voltage applied between the probes C and D (similar definition for $R_{BC,DA}$), and f is a correction factor which is tabulated for different values of $R_{AB,CD}/R_{BC,DA}$ [29]. The contacts between the sample and the silver electrodes have been achieved using a silver paint (Electroquimica DELTA, Resitivity <0.03 Ω cm^{-1}). Two electrodes were polarized using a current source (Keithley 6221), while the potential was measured between the other two probes with a high impedance voltmeter (Keithley 2182A). The measurements were performed at room temperature at three current intensities (50, 100 and 500 μA) and, because the conductivity changes less than 5% with the applied current, we reported the mean value.

To verify that the contact resistance of the silver paint on the sample did not alter the sample conductivity, the measurements were repeated using manual four point resistivity equipment with a SP4 four point probe head (Signatone Corporation), applying a current of 200 μA on the extreme contacts and measuring the potential drop between central contacts. The electrical resistivity was calculated with the expression [31]:

$$\rho = \frac{\pi\delta V}{I f_1 f_2} \quad (2)$$

where V is the applied potential drop, I the measured current, f_1 is a correction factor related to the sample thickness [32], approaching unity as δ approaches zero,

$$f_1 = \ln\left(\frac{\sinh(\delta/s)}{\sinh(\delta/2s)}\right) \quad (3)$$

and f_2 is a correction factor related to the size of the sample [33]:

$$f_2 = \ln(2) + \ln\left(\frac{(D/s)^2+3}{(D/s)^2-3}\right) \quad (4)$$

s being the separation between each contact point (in our test s = 1 mm) and D the diameter of the sample. The resistivity of each sample was measured several times, with different locations of the probes on both faces of the material.

2.2.3. Electrical through-plane resistivity and contact resistance

Several authors have measured or predicted the electrical contact resistance between DL and BP in PEM fuel cells. Some of them studied bipolar plates built with stainless steel [34–36] or graphite [37,38] and the results are important for simulation and models trying to optimize the structure of BP [39] or flow channels [40].

The contact resistance between DL and graphite and the through-plane electrical resistivity of the DL samples were measured using the setup shown in Fig. 1 [41]. In this test, a piece of the mesoporous carbon was located between two plates of graphite (AXF-5QCF from Poco Graphite, Inc.), the assembly was pressurized and the pressure was measured with a load cell (CZC-1000 from Reacción). A potenciostat (Autolab PGSTAT302N, Echochimie) allowed us to apply a potential in the range between −1 mV and

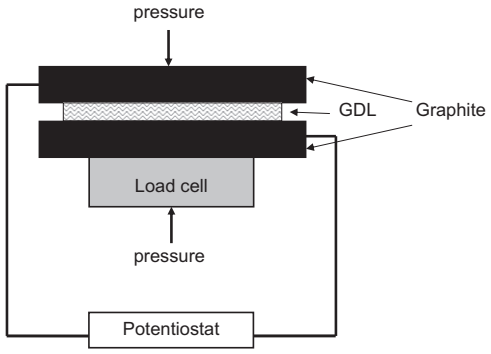

Fig. 1. Scheme of the setup for contact resistance measurements.

+1 mV and the current through the system was measured. The total measured resistance, R_m, obtained from the slope of the current–voltage plot, is then equal to:

$$R_m = R_s + 2R_{c,DL/BP} + R_{b,DL} \quad (5)$$

where R_s is the system resistance, which includes the cables and internal multimeter resistances, $R_{c,DL/BP}$ is the contact resistance between the DL and the BP, and $R_{b,DL}$ is the through-plane bulk resistance of the DL, expressed as:

$$R_{b,CM} = \frac{\rho_{GDL} e_{GDL}}{A_{GDL}} \quad (6)$$

ρ_{GDL}, e_{GDL}, and A_{GDL} being the through plane resistivity, the thickness and the area of the DL, respectively. Eq. (5) can be reorganized,

$$R_m = R_s + \frac{1}{A_{GDL}}\left(2R'_{c,GDL/BP} + \rho_{GDL} e_{GDL}\right) \quad (7)$$

to obtain the contact resistance $R'_{c,GDL/BP} = A_{GDL} R_{c,GDL/BP}$ (units: $\Omega\,cm^2$).

In order to separate the contribution of the contact resistance from the bulk resistance, some authors [42] measure the resistance of samples with different thickness. In our case, we decided to change the contact area. Thus, measuring the resistances of two GDL having different areas, it is possible to determine the contact resistance through Eq. (7),

$$R'_{c,GDL/BP} = \frac{R_{m1} - R_{m2}}{2\left(\frac{1}{A_{GDL,1}} - \frac{1}{A_{GDL,2}}\right)} - \rho_{GDL} e_{GDL} \quad (8)$$

The thickness of the sample was determined with an accuracy of ±1 μm using a thickness meter (Köfer).

2.2.4. Wettability and imbibition

The measurement of the contact angle as a function of time allows the study of the wetting dynamic of aqueous solutions on the carbonous material surface. This is crucial in order to evaluate the feasibility of the aqueous solutions to wet and penetrate the mesoporous material.

Dynamic contact angle measurements of water and aqueous solutions of methanol of different concentrations (1, 2, 3, and 5 M), and pure methanol were performed on four different substrates: our carbonous material carbonized at 800 °C (MC800), commercial Toray® TGPH-090, highly oriented pyrolytic graphite (HOPG), and a glassy carbon (carbonized at 800 °C). The first two materials are porous whereas the two last materials are non porous. We used a contact angle meter (KSV Instruments Ltd., Cam 200) at room temperature, keeping the material rigorously horizontal in front of a camera and following the time evolution of a 1 μL drop deposited on the surface. We determined the mean contact angle as the average between right and left contact angles. Images of the drop were taken each 100 ms for about 30 s and the contact angle was determined by means of the ImageJ software and Drop Analysis plug-in [43]. This program allows drawing the substrate base and drops shape and permit to measure of the angle between the substrate and the radius base of the drop.

Drops imbibition was a fast process in methanol aqueous solutions and for this reason we performed a complementary wetting-imbibition experiment using pure glycerol (J.T. Baker, ACS quality with 0.03% water) in order to slow down the imbibition rate.

2.2.5. Permeability

The hydraulic permeability, K, of a methanol aqueous solution through a monolithic carbonous sample was measured by resorting to Darcy's law (valid for laminar flow) according to [44],

$$Q = KA\frac{\Delta h}{L} \quad (9)$$

where Q is the total discharge of the fluid for a head difference Δh through a sample of surface area A and thickness L.

The MC800 sample was sealed to the end of a capillary tube of internal area a, and kept immersed in a vessel containing 5 M methanol aqueous solution. The capillary was filled with the same solution through the open end and the initial head difference, Δh_0, was recorded. The discharge, as well as the head difference, decreases with time according to $Q = a\Delta h(t)/t$, and the hydraulic permeability can be calculated by integration of Eq. (9), taking into account that the sample area is equal to the capillary area,

$$K = \frac{L}{t}\ln\left(\frac{\Delta h_0}{\Delta h(t)}\right) \quad (10)$$

Once K is determined, the intrinsic permeability, k, which only depends on the sample characteristics is obtained from,

$$k = K\frac{\mu}{\gamma} \quad (11)$$

where μ and γ are the dynamic viscosity and the specific weight of the fluid, respectively.

3. Results and discussion

3.1. Specific surface area and pore size distribution

The results of the structural characterization of the MC800, MC1000, MC800/wC, and MC1000/wC samples are summarized in Table 1. The nitrogen adsorption–desorption isotherms of the MC800 sample is illustrated in Fig. 2, where an increase of the nitrogen adsorbed volume in the low relative pressure and a hysteresis loop at high relative pressure, can be observed. According to the IUPAC classification, the isotherm is of type-IV, and it has a hysteresis loop of type-H1 [28]. Similar isotherms were obtained for the MC1000 sample and the analysis using the BET equation indicates that the mesoporous carbon samples have a moderate specific surface area (670–750 $m^2\,g^{-1}$) as compared with OMC [45], while the results summarized in Table 1 are similar to those reported for similar materials [46,47].

Table 1
Structural properties of the mesoporous carbon samples.

Sample	BET area ($m^2\,g^{-1}$)	Total pore volume ($cm^3\,g^{-1}$)	Micropore volume ($cm^3\,g^{-1}$)
MC800	700	1.14	0.20
MC1000	670	0.95	0.21
MC800/wC	742	0.99	0.20
MC1000/wC	690	0.96	0.19

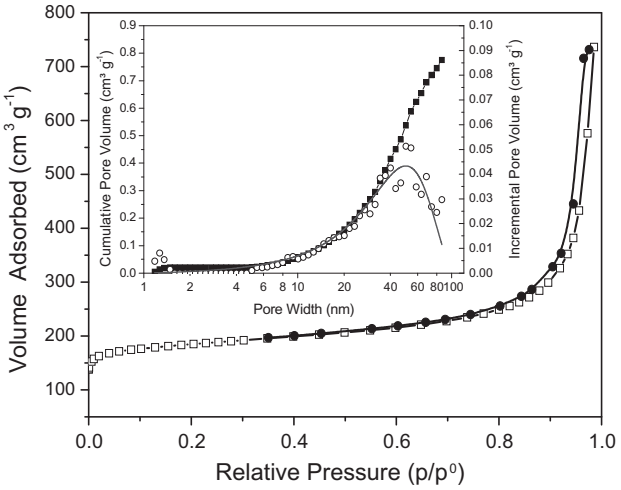

Fig. 2. Nitrogen adsorption isotherm and pore size distribution of the mesoporous carbon (800 °C).

The type-H1 hysteresis loop at high relative pressure is associated to mesoporous materials with a relatively narrow distribution of pore size, although wider than that observed in OMC. The total pore volume (at $p/p^{\circ} = 0.98$) is slightly higher for the MC800 sample as compared to MC1000, while the pore size distributions are similar for both samples. The *t*-plot micropore volume is similar for all the samples.

The pore size distribution (inset in Fig. 2), calculated using DFT model from the isotherm data, assuming slit pore geometry, shows a maximum of the pore distribution around 40–60 nm for MC800 and MC1000 (not shown). The micro (<2 nm) and mesoporosity (2–50 nm) of the MC is attributed to its structure, which consists of clusters of porous uniform spheres in a fairly regular array [6], as illustrated by the SEM photograph in Fig. 3a.

In summary, the pore size distribution of our MC is quite different from that reported by Yoshizawa et al. [48] for carbon-paper (Carbel CFP300) and carbon-cloth (Carbel CL), both having a macroporous layer with porosity around 100 nm, and other layer with capillaries. The size of the capillaries is around 50 μm for carbon-paper and a broad pore distribution from 5 to 100 μm for carbon-cloth. In order to improve the GDL performance under humidified conditions or in case of anodic GDL in DMFC, our MC can be fabricated with capillaries having sizes of the order of microns [10]. A micrograph of the MC800/wC sample showing the capillary distribution is shown in Fig. 3b.

The roughness of the samples was in the range 70–80 nm as determined with the surface profiler, in good agreement with the nano-roughness determined by AFM (95 nm).

3.2. Electrical resistivity of the mesoporous carbon

The measured resistivities for different GDL in the in-plane direction are summarized in Table 2, along with results reported in the literature. It can be observed that the resistivity of MC measured with the van der Pauw method is lower that determined by the in line 4 point method, probably as a consequence of the partial penetration of the silver paint used as contacts in the first method. Therefore, the results obtained with the in line 4 point method should be considered as the most reliable ones.

The lower resistivity of the MC1000 as compared to MC800 could be explained by the fact that the pyrolysis of the phenolic resin leads to the destruction of the polymeric network and the formation of hexagonal carbon layers which expands with increasing temperature reaching complete graphitization above 1500 °C. Due to this graphitization process the electrical conductivity of the MC, which is similar to carbon aerogel, increases dramatically in the temperature region 500–800 °C, increases moderately above 800 °C, and reaches a plateau at higher temperatures [49]. Thus,

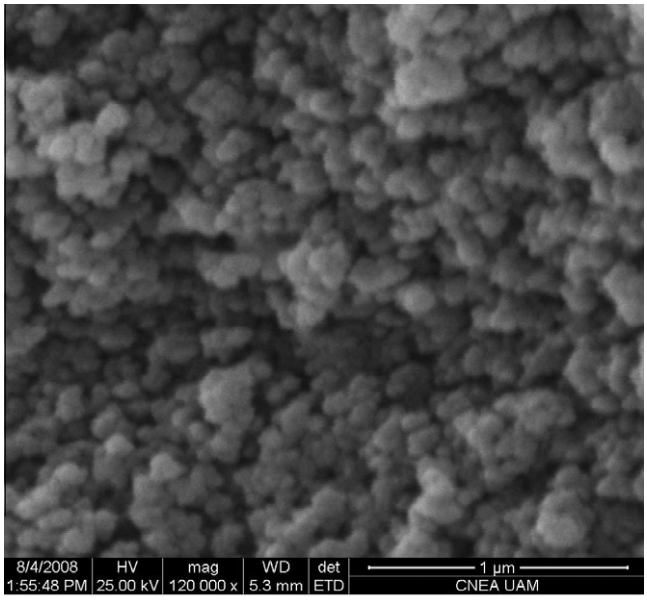

Fig. 3. SEM images of MC800 (a) and MC800/wC (b).

Table 2
In-plane electrical resistivity of different carbonous materials used as GDL.

Sample	Thickness (μm)	ρ (mΩ cm)	Technique	Refs.
MC800	254	135	van der Pauw	This work
		215	4 in-line probes	This work
MC1000	316	35	van der Pauw	This work
		38	4 in-line probes	This work
MC800/wC	282	270	4 in-line probes	This work
MC1000/wC	298	73	4 in-line probes	This work
Toray 060	190	6.3	4 in-line probes	This work
		5.5[a]		[42]
		5.8		[54]
Toray 090	280	6.2	4 in-line probes	This work
		5.6		[54]
Toray 120	370	4.7		[54]
		4.8–7.2[b]		[55]
Carbon cloth	380	9		[42,54]

[a] Average value between machine direction and cross-machine direction (4.4–6.5 mΩ cm).
[b] The lowest value corresponds to 0% PTFE, and the highest one to 40% PTFE.

increasing the final carbonization temperature results in a number of changes in the material, including not only an enhancement of its electrical conductivity, but also shrinkage (density increase) [50], reduction of the hydrogen and oxygen content [49,51], and microcrystalline size [52].

The resistivity values for MC1000 indicate that it would be an adequate material for fuel cells as well as a support for electrodeposited catalysts [11], provided that the main contribution to the total resistance of the cell is the contact resistance that will be discussed below.

The resistivity of a MC having capillaries 15 μm in diameter (crossing the sample in the normal direction) and carbonized at 1000 °C (MC1000/wC) [10] is also reported in Table 2. Its resistivity is almost a factor 2 higher than that measured for MC1000, which is consequence of the reduction of the surface area of the MC sample due to the presence of the capillaries, estimated in 40% of the geometric area.

We assumed that the prepared MC is completely isotropic [53], meaning that in-plane and through-plane conductivities are equal. In Table 3 we compared the through-plane resistivity of the MC with those reported for commercial available carbon-paper and carbon-cloth [42,54,55].

The effect of Teflon® content on the resistivity is illustrated in Tables 2 and 3 for Toray TGP-H-120 by the results by Lobato et al. [55]. In plane and through-plane resistivity increase by a factor 1.5 and 2.8, respectively, when the Teflon® content increases from 0% to 40%. Therefore, the resistivities of our MC materials should be compared with those corresponding to commercial GDLs having 0% PTFE.

The results of in-plane resistivity (Table 2) show that MC1000 is between 4 and 7 times more resistive than Toray carbon-paper and carbon cloth, and the difference is more than a factor 10 for MC1000/wC. The lower resistivity of the commercial GDL is probably due to the fact that this material is made of carbon fibers mostly oriented in the in-plane direction such that conductivity occurs in that direction.

However, when the through-plane resistivity is compared (Table 3), it is concluded that the MC1000 material, without and with capillaries, has lower resistivity than the commercial GDLs. Thus, it is expected that the mesoporous carbon prepared by the procedure described here would enhance the efficiency of fuel cells, because the conduction of electrons from the catalytic zone to the current collector is mainly achieved in the transversal direction of the cell. Nevertheless, this conclusion should be confirmed by the analysis of the contact resistance between MC and BP, addressed in the next section.

The electrical resistivity of our MC can be also compared with OMC prepared by Joo et al. [56] from phenanthrene and sucrose by nanoreplication method using mesoporous silica as a template. These authors reported sheet resistances of 54 and 202 $m\Omega\,cm^{-2}$ for phenantrene and sucrose OMC, respectively, well above the values 5.5 and 1.2 $m\Omega\,cm^{-2}$ obtained in this work for MC800 and MC1000, respectively. This result could be associated to a lower degree of graphitization (higher oxygen content) or a thinner carbon walls in the OMC prepared with a silica template, as compared to the monolithic MC.

Table 3
Through-plane electrical resistivity of different carbonous materials.

Sample	ρ (mΩ cm)	Refs.
MC800	215[a]	This work
MC1000	38[a]	This work
MC1000/wC	73[a]	This work
Toray 060	80	[42,54]
Toray 090	80	[54]
Toray 120	80	[54]
Toray 120	95–270[b]	[55]
Carbon cloth	132	[54]

[a] Assumed values.
[b] The lowest value corresponds to 0% PTFE, and the highest one to 40% PTFE.

3.3. Contact resistance

Fig. 4 shows the behavior of the contact resistance of graphite BP with MC800, MC1000/wC, Toray-TGPH-090, and carbon cloth, determined by using the setup of Fig. 1 and Eq. (8), as a function of the applied pressure. We assumed that the through-plane resistivity of the MC samples is independent on pressure because of their high compression modulus. For carbon-paper GDL, Nitta et al. [38] and Kleemann et al. [57] have shown that the through-plane resistivity is highly compression dependent. In particular the resistivity of Toray TGP-H-060 decreases by a factor of six between 1 and 5 bar, but it reduces to the half increasing the pressure from 5 to 15 bar [57]. Therefore, in the calculation of the contact resistance of Toray-TGP-H-090 using Eq. (8) we have assumed that the product $\rho_{GDL}{\cdot}e_{GDL}$, which contributes in a small proportion to the measured total resistance, remains constant.

The pressure dependence of the contact resistance of Toray-TGP-H-090 is similar to that reported by other authors for this carbon-paper GDL with and without Teflon® loading [42], for carbon-cloth GDL [58], and for other GDLs [35,37,58–60]. A quantitative comparison of the Toray and carbon-cloth contact resistance with published results is not possible because other materials different of graphite, such as copper or stainless steel, have been used as BP. The values of contact resistance reported in Fig. 4 for Toray TGP-H-090 without Teflon agree with those reported by Mathias et al. [42] for Toray TPG-H-060 with 3.5% Teflon® at pressures up to 12 bar, and almost a factor 2 higher than those of Toray TPG-H-060 with 0% Teflon®. Probably, the differences are in part due to different roughness of the graphite BP.

The decrease of the contact resistance of MC800 with increasing pressure follows the same tendency observed for carbon-paper and carbon-cloth, but it is much more pronounced at pressures up to 10 bar. Above 15 bar the contact resistance of graphite/MC800 lies below that of graphite/Toray, and reaches values remarkable low at pressures above 20 bar. The contact resistance graphite/MC1000/wC is much lower than that of graphite/carbon cloth above 15 bar, although even at pressures above 25 bar remains higher than that of Toray. However, the slope of the curve contact resistance vs. pressure for graphite/MC1000/wC would indicate that at high pressures the contact resistance could reach values similar to graphite/Toray.

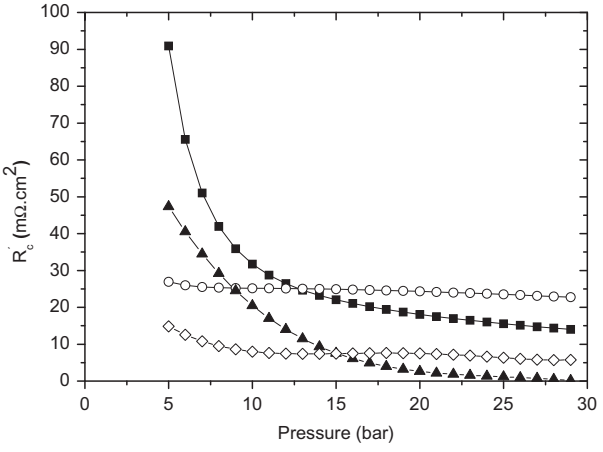

Fig. 4. Contact resistance as a function of pressure for MC 800 (▲); MC1000/wC (■), Toray-TGPH-090 (◇); carbon cloth (○).

The difference between MC800 and MC1000/wC contact resistances, which remain constant at pressures above 15 bar, is due in part to the reduction of the contact area with the BP of the MC with capillaries.

These results are interesting in relation with the use of MC as GDL in PEM fuel cell, where the stack is assembled at pressures between 10 and 20 bars for an optimal performance [61]. The pressure behavior of the contact resistance for MC and Toray could be explained by differences in their compression modules. The Young's modulus of a MC similar to that used in this study is around 6.6 GPa as determined by nanoidentation [62], while the macroscopic determination of Young's modulus yields to values between 1.8 GPa (stress lower than 3 MPa) up to 4.8 GPa (stress higher than 3 MPa) [63]. This module is assumed to be isotropic in MC, while the mechanical properties of Toray paper are highly anisotropic. According to Kleeman et al. [57], Toray carbon-paper in the GDL plane is much stiffer than in the through-plane direction, where the porosity dominates the mechanical properties. For this reason, the Young's modulus in the material plane is in the order of 7 GPa, that is, of the order of the carbon fiber that forms the material, but it decreases to tens of MPa in the transverse direction. A recent analysis of the mechanical properties of Toray TGP-H-060/090 shows that at low strain the through-plane Young's modulus changes between 1.4 MPa and 14 MPa, it remains constant at (14 MPa) at intermediate strain and finally increases with the strain at large strains reaching values up to 30 MPa [64]. Therefore, compared with MC, Toray carbon paper are relatively soft material, and carbon cloth is still softer, that is, it deforms increasing the contact area with the BP at low pressure. For this reason the contact resistance in Fig. 4 for carbon-paper and carbon cloth is almost constant at pressures above 5 bar.

The high contact resistance values of the MC materials at low pressures and the sharp decrease with increasing pressure could be explained considering its high compression modulus as compared with commercial GDL. Thus, a pressure of 10 bar (1 MPa) applied on a MC layer 300 μm in thickness, will reduce its thickness in approximately 160 nm, which is of the order of magnitude of the MC roughness reported above. The decrease of the contact resistance between carbon and BP with increasing pressure due to smoothing of the rough surface, which in turns increase the real contact area has been recently discussed by Mench and coworkers [65,66].

3.4. Wettability and imbibition

Contact angles for water and 1 M methanol aqueous solution droplets on the Toray TGPH-090, HOPG and glassy carbon remain essentially constant 30 s after contacting the surface, while in the case of MC contact angles decrease very rapidly and the imbibition on dry surfaces is almost complete in few seconds. The imbibition becomes slower when the MC is partially wet, as shown in Fig. 5, which shows the imbibition of a second droplet on the same region where a first drop penetrated. Any significant difference was observed between the imbibition of MC800 and MC1000 samples provided that the surfaces were clean and dry. In Table 4 are summarized the contact angles determined for all the substrates.

Table 4
Contact angle of water and 1 M methanol aqueous solution on different carbon surfaces.

Sample	Contact angle (water)	Contact angle (1 M methanol)	Refs.
HOPG	85 ± 4	74 ± 2	This work
Glassy carbon	76 ± 4	70 ± 4	This work
Toray TGP-H-090	155 ± 5	135 ± 5	This work
Toray TGP-H-090	104 ± 4		[68]
Toray TGP-H-060[a]	135		[42]
Toray TGP-H-120	115/30		[67]
MC800[b]	74 ± 2	68 ± 2	This work
MC	141		[69]
MC	81		[70]
OMC	79.1 ± 1.5		[71]
OMC	38.4		[72]

[a] Advancing/receding.
[b] Initial values ($t = 0$).

Glassy carbon and HOPG contact angles are slightly lower than 90° indicating a hydrophilic behavior and they remain constant in time for both fluids as expected for a non-porous structure.

Fluid imbibition was not observed for Toray TPG-H-090, a porous carbon paper composed of carbon fibers without Teflon® coating. The hydrophobic nature of the carbon paper, as revealed by the measured contact angles for water and 1 M methanol solution, explains why the droplets do not penetrate the material when pressure is not applied. Thus, Benziger et al. [67] concluded that a minimum pressure of 1200 Pa should be initially applied to an initially wet Toray TPG-H-120 carbon paper for permitting water to flow through.

The contact angle values reported for Toray TPG-H-090 and other similar untreated Toray papers spread over a wide range, although in all cases are higher than 100° [42,67,68]. Gurau et al. [69] have noted that large contact angle values cannot be explained by the presence of hydrophobic agents inside the carbon paper GDL pores, but rather by the contribution of GDL surface roughness above approximately 1 μm.

In the case of the MC the surface roughness is much lower than this threshold value, consequently, the initial contact angles are much lower than those observed for Toray TGP-H-090, and the material is clearly hydrophilic. Such a behavior has been reported for similar MC and OMC having smaller pore sizes [70–73], with the exception of a recent study by Cao et al. [70], who have observed a super-hydrophobic behavior on a MC prepared from phenol-formaldehyde resins using Pluronic 127 as a template. It should be noted that this MC have a uniform pore size of 2.2 nm and a pore volume of 0.12 $cm^3\ g^{-1}$, which apparently leads to a completely different wettability behavior.

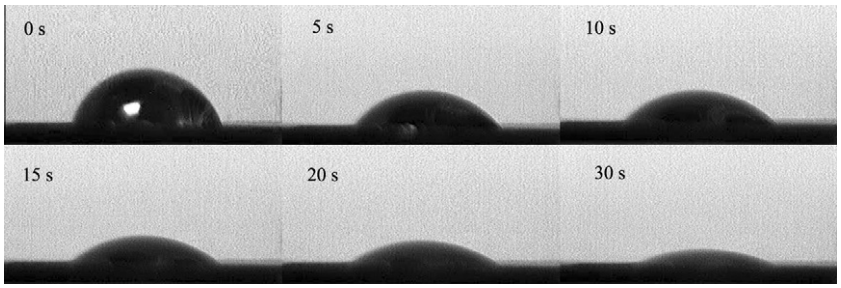

Fig. 5. Time evolution of a second water droplet onto mesoporous carbon substrate MC800.

A more detailed analysis of the initial dynamic of the contact angle in MC is shown in Fig. 6, where it is clearly observed that methanol aqueous solutions in the range 2–3 M barely wet the MC surface, while more concentrated methanol solutions, including pure methanol, spread and penetrate in the MC without droplet formation.

Our results show a similar dynamic as compared to those published by Clarke et al. [74], who studied the spreading and imbibition of water and glycerol aqueous solutions (having almost half the surface tension of water) on a microporous filter membrane, made from mixed cellulose ester, with a nominal pore diameter from 0.1 to 0.65 μm. From the variation of the volume of the drop as a function of time these authors could verify the validity of a model describing the spreading and imbibition of liquids on porous surfaces, having into account the surface tension of the fluid. They observed a large difference between the low and high surface tension liquids, with the imbibition process being more than two orders of magnitude quicker for the lower surface tension liquid.

The surface tension of pure water is 72.01 mN m^{-1}, and decrease sharply with the methanol concentration, reaching half of this value for a methanol solution with a methanol concentration around 12 M, and 22.51 mN m^{-1} for pure methanol [75]. Thus, the relaxation of the contact angle of concentrated methanol solutions is expected to occur over a period shorter than 10 ms, which is beyond the limit that could be achieved with our experimental setup.

Starov [76] developed a model that considers, simultaneously, the increase of the base radius of the drop during the spreading and the decrease of the base radius of the drop due to imbibition. Under partial wetting the process occurs in three defined stages. In the first stage the contact angle decreases while the base drop radius increases. The base drop radius remains constant while the contact angle decreases linearly with time during the second stage. Finally, in the third stage the base drop radius decreases until the drop disappears and the contact angle remains constant. Hilpert and Ben-David [77] developed a detailed model of wetting and imbibition, which recognizes the three stages described by Starov, denoted as increasing (IDA), constant (CDA), and decreasing (DDA) drawing area.

The three stages are not observed in the case of the spreading and imbibition of low viscosity liquids, like methanol aqueous solutions, but when glycerol is used as test fluid these stages can be visualized, as depicted in Fig. 7. Although, characteristic parameters of the mesoporous material can be determined by fitting the time dependence of the contact angle or the radius of the drop, a detailed analysis of the wettability and imbibition of liquids in mesoporous carbon are out of the scope of this work and it will be undertaken in a forthcoming study.

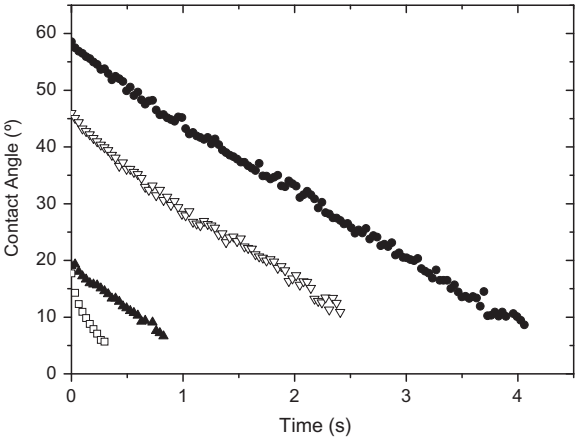

Fig. 6. Dynamic contact angle for water and methanol aqueous solutions on MC1000: (♦) water; (▽) 1 M methanol; (▲) 2 M methanol; (□) 3 M methanol.

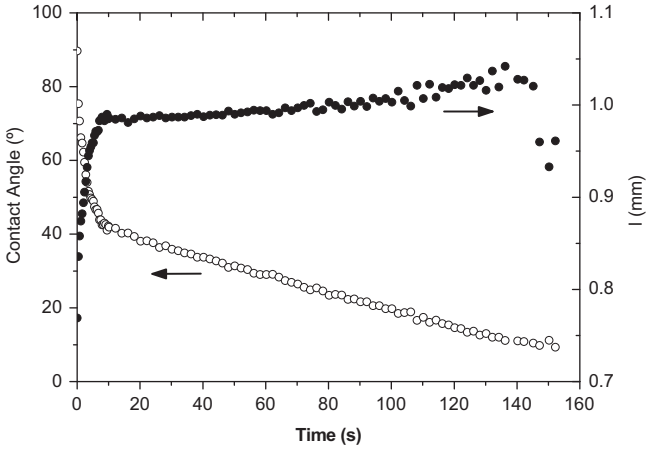

Fig. 7. Dynamic contact angle and radius of a glycerol drop on MC800.

3.5. Permeability

The measured hydraulic permeability of a 5 M methanol aqueous solution at 20 °C was $K = (1.1 \pm 0.1) \times 10^{-10}$ m s^{-1}. From this value, and considering $\mu = 1.5 \times 10^{-3}$ Pa s, and $\gamma = 9.53$ kN m^{-3} for a 5 M methanol aqueous solution [78], the calculated intrinsic permeability was $k = (1.7 \pm 0.2) \times 10^{-17}$ m^2.

The intrinsic permeability of the carbonous material can be correlated to a characteristic particle diameter, d, and the porosity, ε, through the Kozeny–Carman equation [79,80], which in the case of approximately spherical particles with a narrow size distribution, adopts the form,

$$k = \frac{d^2 \varepsilon^3}{36 C_k (1-\varepsilon)^2} \tag{12}$$

where $C_k = c\tau^2$, depends on the Kozeny constant, c, which accounts for a shape factor of the pores and the tortuosity, τ, of the sample. The experimental results indicate that $C_k \approx 5$ [44,80,81] in the porosity range 0.26–0.80 for packing beds, even in the case of bidisperse spherical particles.

Because the sample porosity can be estimated according to:

$$\varepsilon = \frac{V_p}{V_p + V_C} \tag{13}$$

where V_p is the specific pore volume (1.14 cm^3 g^{-1}) obtained from the BET isotherm and $V_C = 0.690$ cm^3 g^{-1} is the specific volume of the compact carbon, as measured in a previous work [62]. Thus, the porosity of the mesoporous carbon is $\varepsilon = 0.62$, a value which is within the range of validity of the Kozeny–Carman equation.

By using Eq. (5) an average particle diameter $d = (43 \pm 13)$ nm was calculated. The agreement with the particle size previously reported, around 60–80 nm, observed from SEM images [11], is quite reasonably taking into account that the empirical constant in Eq. (5) was obtained from experimental data for non-consolidated materials with macroporosity.

On the other hand, Eq. (5) is also employed in the original Kozeny form, which assumes a porous media formed by parallel cylindrical capillaries in the flow direction. In that case the diameter of the capillaries, d_p, replace the particle diameter in Eq. (5), and the result (43 nm) is coherent with the pore distribution shown in Fig. 2.

The intrinsic permeability of Toray TGP-H-090 carbon-paper (porosity = 0.78), is 8.3×10^{-12} m^2 [82], that is, more than five orders of magnitude that of our MC, as expected by the higher pore size of the carbon paper. Therefore, it is important to estimate the performance of the MC as diffusion layer in the anode of DMFC by calculating the number of moles of methanol reaching the surface of the catalyst layer after permeating through a layer of MC 200 μm in thickness. Using Darcy's law (Eq. (9)), and assuming a head difference of 10 cm and complete conversion of methanol to CO_2 on the anode (six electrons process) a 5 M methanol solution would be able to sustain a current density of 15 mA cm^2. For pure methanol the current density under the same conditions would rise up to 74 mA cm^2, which is close to the state of the art for passive DMFC [83]. The performance could be also improved by increasing the head difference or, preferably, by using the MC with capillaries for providing extra large pores for liquid permeability, increasing the intrinsic permeability up to 1.8×10^{-10} m^2 [10].

4. Conclusions

A monolithic mesoporous carbon material has been prepared from a resorcinol-formaldehyde resin using a cationic polyelectrolyte poly(diallyldimethylammonium chloride) as a soft template and carbonization at temperatures between 800 and 1000 °C. The material exhibits a moderate specific surface area (670–750 m^2 g^{-1}) and the pore size distribution shows a maximum around 45 nm, while the specific surface area indicates the presence of micropores (<2 nm), suggesting a structure consisting of clusters of porous uniform spheres in a fairly regular array, as shown by SEM analysis.

The electrical resistivity of the mesoporous carbon prepared at 1000 °C is higher than that of the material carbonized at 800 °C due to the increase of the degree of graphitization at higher temperatures. The resistivity of MC1000 is several times higher than the in-plane resistivity of Toray carbon-paper and carbon cloth, but it is much lower than the through-plane resistivity of the commercial GDLs. The electrical resistivity of our MC it is also lower than other OMC prepared from phenanthrene and sucrose by nanoreplication method using mesoporous silica as a template. These electrical characteristics of the MC combined with its relatively high superficial area, indicate that the monolithic carbon could be good candidate as support for metal catalyst layers.

The contact resistance graphite/MC at low pressure is higher than that observed for graphite/Toray and graphite/carbon-cloth, but it decreases sharply with pressure, and above 15 bar the graphite/MC800 contact resistance is lower than that of commercial GDL, reaching values remarkable low at pressures above 20 bar. The dramatic reduction of the contact resistance of the MC can be explained resorting to its low roughness and an adequate compression modulus. In summary, the electrical properties of MC meet the requirements to be employed as GDL in PEM fuel cell with stack assembled at pressures above 15 bar.

The wettability and imbibition properties of the mesoporous carbon by aqueous methanol depend on the methanol concentration, due to the reduction of the surface tension with increasing methanol content. The rapid spreading and imbibition of concentrated methanol solutions in MC is interesting considering the possibility of using this material in passive direct methanol fuel cells. Also, the permeability of aqueous methanol through MC is adequate for the low flow level used in micro fuel cells. Both, imbibition and permeability could be tuned by controlling the pore size during the carbonization process and the pore hydrophobicity.

In a future work, this MC material will be used in a direct methanol single cell in order to compare its behavior as GDL and catalyst support, and analyze the micro fluid dynamics of methanol penetration and gaseous CO_2 drain.

Acknowledgements

Financial support from Agencia Nacional de Promoción Científica y Tecnológica (PICT 2097 and PAE 36985) is gratefully acknowledged. Surface analysis characterization was performed on Laboratorio de Microscopia Electrónica of CAC with the help of P. Bozzano, A. Dominguez and P. Reynoso Peitsch, while Dr. M. Reinoso (Surface Group, Tandar) helps us with the roughness measurements. The collaboration of J. Bonaparte from MEMS group of CNEA is gratefully acknowledged. MMB and HRC are members of the CIC of CONICET. YRJT thanks CONICET for his fellowship.

References

[1] A. Kundu, J.H. Jang, J.H. Gil, C.R. Jung, H.R. Lee, S.H. Kim, B. Ku, Y.S. Oh, J. Power Sources 170 (2007) 67–78.
[2] W. Qian, D.P. Wilkinson, J. Shen, H. Wang, J. Zhang, J. Power Sources 154 (2006) 202–213.
[3] J.-H. Wee, J. Power Sources 161 (2006) 1–10.
[4] T. Schaffer, V. Hacker, J.O. Besenhard, J. Power Sources 153 (2006) 217–227.
[5] F. Achmad, S.K. Kamarudin, W.R.W. Daud, E.H. Majlan, Appl. Energy 88 (2011) 1681–1689.
[6] A. Taguchi, F. Schüth, Micropor. Mesopor. Mater. 77 (2005) 1–45.
[7] H. Chang, S.H. Joo, C. Pak, J. Mater. Chem. 17 (2007) 3078–3088.
[8] J.Y. Lee, Y.H. Yun, S.W. Park, S.D. Kim, S.C. Yi, W.J. Kim, Micropor. Mesopor. Mater. 134 (2010) 1–7.
[9] Z. Lei, L. An, L. Dang, M. Zhao, J. Shi, S. Bai, Y. Cao, Micropor. Mesopor. Mater. 119 (2009) 30–38.
[10] M.M. Bruno, H.R. Corti, J. Balach, N.G. Cotella, C.A. Barbero, Funct. Mater. Lett. 2 (2009) 135–138.
[11] M.M. Bruno, E.A. Franceschini, G.A. Planes, H.R. Corti, J. Appl. Electrochem. 40 (2010) 257–263.
[12] G. Ramos-Sánchez, M.M. Bruno, Y.R.J. Thomas, H.R. Corti, O. Solorza-Feria, Int J. Hydrogen Energy 37 (2012) 31–40.
[13] L. Cindrella, A.M. Kannan, J.F. Lin, K. Saminathan, Y. Ho, C.W. Lin, J. Wertz, J. Power Sources 194 (2009) 146–160.
[14] A. Oedegaard, C. Hebling, A. Schmitz, S. Møller-Holst, R. Tunold, J. Power Sources 127 (2004) 187–196.
[15] J.-Y. Park, H.-T. Kim, E.S. Lee, I.-H. Son, S. Han, Int. J. Hydrogen Energy 34 (2009) 8257–8262.
[16] C. Lin, T. Wang, F. Ye, Y. Fang, X. Wang, Electrochem. Commun. 10 (2008) 255–258.
[17] M. Glora, M. Wiener, R. Petričvić, H. Pröbstle, J. Fricke, J. Non-Cryst. Solids 285 (2001) 283–287.
[18] Y. Meng, D. Gu, F. Zhang, Y. Shi, L. Cheng, D. Feng, Z. Wu, Z. Chen, Y. Wan, A. Stein, D. Zhao, Chem. Mater. 18 (2006) 4447–4464.
[19] K. Kraiwattanawong, N. Sano, H. Tamon, Carbon 49 (2011) 3404–3411.
[20] A.K. Sahu, K.G. Nishanth, G. Selvarini, P. Sridhar, S. Pitchumani, A.K. Shukla, Carbon 47 (2009) 102–108.
[21] S. Tanaka, N. Nakatani, A. Doi, Y. Miyake, Carbon 49 (2011) 3184–3189.
[22] P. Li, Y. Song, Q. Guo, J. Shi, L. Liu, Mater. Lett. 65 (2011) 2130–2132.
[23] H.-P. Lin, C.-Y. Chang-Chien, C.-Y. Tang, C.-Y. Lin, Micropor. Mesopor. Mater. 93 (2006) 344–348.
[24] M.V. Williams, E. Begg, L. Bonville, H.R. Kunz, J.M. Fenton, J. Electrochem. Soc. 151 (2004) A1173–A1180.
[25] P.M. Wilde, M. Mndle, M. Murata, N. Berg, Fuel Cells 4 (2004) 180–184.
[26] M.V. Williams, H.R. Kunz, J.M. Fenton, J. Electrochem. Soc. 151 (2004) A1617–A1627.
[27] M.M. Bruno, N.G. Cotella, M.C. Miras, C.A. Barbero, Colloids and Surface A 362 (2010) 28–32.
[28] F. Rouquerol, J. Rouquerol, K. Sing, Adsorption by Powders and Porous Solids, Academic Press, San Diego, 1999.
[29] L.J. van der Pauw, Philips Res. Rep. 13 (1958) 1–9.
[30] Standard Test Methods for Measuring Resistivity and Hall Coefficient and Determining Hall Mobility in Single-Crystal Semiconductors, ASTM, F 76–86 R.
[31] D.K. Schroeder, Semiconductor Material and Device Characterization, John Wiley & Sons, Ltd., 1990.
[32] A. Uhlir Jr., Bell Syst. Tech. J. 34 (1955) 105–128.
[33] F.M. Smits, Bell Syst. Tech. J. 37 (1957) 711–718.
[34] H. Wang, M.A. Sweikart, J.A. Turner, J. Power Sources 115 (2003) 243–251.
[35] M.S. Ismail, T. Damjanovic, D.B. Ingham, M. Pourkashanian, A. Westwood, J. Power Sources 195 (2010) 2700–2708.
[36] J. Ihonen, F. Jaouen, G. Lindbergh, G. Sundholm, Electrochim. Acta 46 (2001) 2899–2911.
[37] V. Mishra, F. Yang, R. Pitchumani, J. Fuel Cell Sci. Technol. 1 (2004) 2–9.
[38] I. Nitta, T. Hottinen, O. Himanen, M. Mikkola, J. Power Sources 171 (2007) 26–36.
[39] P. Zhou, C.W. Wu, G.J. Ma, J. Power Sources 159 (2006) 1115–1122.

[40] A. Higier, H. Liu, Int. J. Hydrogen Energy 36 (2011) 1664–1670.
[41] N. Cunningham, M. Lefèvre, G. Lebrun, J.-P. Dodelet, J. Power Sources 143 (2005) 93–102.
[42] M. Mathias, J. Roth, J. Fleming, W. Lehnert, Chapter 46, Diffusion media materials and characterization. Handbook of Fuel Cells, Fundamentals, Technology and Applications, vol. 3, Fuel Cell Technology and Applications, John Wiley & Sons, Ltd., 2003.
[43] A.F. Stalder, G. Kulik, D. Sage, L. Barbieri, P. Hoffmann, Colloids Surf. A 286 (2006) 92–103.
[44] S. Lister, N. Djilali, Two-phase transport in porous gas diffusion electrodes. In: Sundén, B., Faghri, M. (Eds.), Transport Phenomena in Fuel Cells, WIT Press, Southampton, UK, 2005, p. 181–182 (Chapter 5).
[45] E. Antolini, Appl. Catal. B 88 (2009) 1–24.
[46] J. Marie, S. Berthon-Fabry, M. Chatenet, E. Chainet, R. Pirard, N. Cornet, P. Achard, J. Appl. Electrochem. 37 (2007) 147–153.
[47] C. Arbizzani, S. Beninati, E. Manferrari, F. Soavi, M. Mastragostino, J. Power Sources 161 (2006) 826–830.
[48] K. Yoshizawa, K. Ikezoe, Y. Tasaki, D. Kramer, E.H. Lehmann, G.G. Scherer, J. Electrochem. Soc. 155 (2008) B223–B227.
[49] C.L. Liu, W.S. Dong, J.R. Song, L. Liu, Mater. Sci. Eng. A 459 (2007) 347–354.
[50] N. Job, R. Pirard, J. Marien, J.P. Pirard, Carbon 42 (2004) 619–628.
[51] E. Fitzer, W. Schäfer, Carbon 8 (1970) 353–364.
[52] R. Franklin, Proc. Royal Soc. A209 (1951) 196–218.
[53] G.M. Jenkins, K. Kawamura, Polymeric Carbons – Carbon Fiber, Glass and Char, Cambridge University Press, Cambridge, 1976.
[54] F. Barbir, PEM Fuel Cells, Theory and Practice, Elsevier Academic Press, London, 2005. p. 94.
[55] J. Lobato, P. Cañizares, M.A. Rodrigo, C. Ruiz-Lopez, J.J. Linares, J. Appl. Electrochem. 38 (2008) 793–802.
[56] S.H. Joo, C. Pak, D.J. You, S.A. Lee, H.I. Lee, J.M. King, H. Chang, D. Seung, Electrochim. Acta 52 (2006) 1618–1626.
[57] J. Kleemann, F. Finsterwalder, W. Tillmetz, J. Power Sources 190 (2009) 92–102.
[58] S. Escribano, J.F. Blachot, J. Ethève, A. Morin, R. Mosdale, J. Power Sources 156 (2006) 8–13.
[59] T. Matsuura, M. Kato, M. Hori, J. Power Sources 161 (2006) 74–78.
[60] Y. Zhou, G. Lin, A.J. Shih, S.J. Hu, J. Power Sources 163 (2007) 777–783.
[61] W.R. Chang, J.J. Hwang, F.B. Weng, S.H. Chan, J. Power Sources 166 (2007) 149–154.
[62] M.M. Bruno, N.G. Cotella, M.C. Miras, T. Koch, S. Seidler, C. Barbero, Colloids Surf. A 358 (2010) 13–20.
[63] M.M. Bruno, Ph.D. Thesis, University of Rio Cuarto, 2007.
[64] P.A. García-Salaberri, M. Vera, R. Zaera, Int. J. Hydrogen Energy 36 (2011) 11856–11870.
[65] T. Swamy, E.C. Kumbur, M.M. Mench, J. Electrochem. Soc. 157 (2010) B77–B85.
[66] T. Swamy, E.C. Kumbur, M.M. Mench, Electrochim. Acta 56 (2011) 3060–3070.
[67] J. Benziger, J. Nehlsen, D. Blackwell, T. Brennan, J. Itescu, J. Membr. Sci. 261 (2005) 98–106.
[68] J.D. Fairweather, P. Cheung, D.T. Schwartz, J. Power Sources 195 (2010) 787–793.
[69] V. Gurau, M.J. Bluemle, E.S. De Castro, Y.-M. Tsou, J.A. Mann Jr., T.A. Zawodzinski Jr., J. Power Sources 160 (2006) 1156–1162.
[70] Y.J. Cao, M. Liu, L. Gan, Y. Lv, Z. Xu, Z. Hao, H. Liu, L. Chen, Adv. Mater. Res. 239–242 (2011) 3190–3193.
[71] H. Tang, S.P. Jiang, J. Phys. Chem. C 112 (2008) 19748–19755.
[72] L. Wang, Y. Zhao, K. Lin, X. Zhao, Z. Shao, Y. Di, Z. Sun, X. Cao, Y. Zou, D. Jiang, L. Jiang, F.S. Xiao, Carbon 44 (2006) 1298–1352.
[73] C.X. Guo, F.P. Hu, X.W. Lou, C.M. Li, J. Power Sources 195 (2010) 4090–4097.
[74] A. Clarke, T.D. Blake, K. Carruthers, A. Woodward, Langmuir 18 (2002) 2980–2984.
[75] G. Vazquez, E. Alvarez, J.M. Navaza, J. Chem. Eng. Data 40 (1995) 611–614.
[76] V.M. Starov, Adv. Coll. Interfase Sci. 111 (2004) 3–27.
[77] M. Hilpert, A. Ben-David, Int. J. Multiphase Flow 35 (2009) 205–218.
[78] R.C. Weast, CRC Handbook of Chemistry and Physics, 69th ed., CRC Press, Boca Raton, FL, USA, p. D-238.
[79] J. Kozeny, Stizungsber Akad. Wiss. Wien 136 (1927) 271–306.
[80] P.C. Carman, Trans. Inst. Chem. Eng. 15 (1937) 150–167.
[81] Y. Li, C.W. Park, Ind. Eng. Chem. Res. 37 (1998) 2005–2011.
[82] J.T. Gostick, M.W. Fowler, M.A. Ioannidis, M.D. Pritzker, Y.M. Volfkovich, A. Sakars, J. Power Sources 156 (2006) 375–387.
[83] L. Feng, J. Zhang, W. Cai, Liangliang, W. Xing, C. Liu, J. Power Sources 196 (2011) 2750–2753.